Motions of a Floating Body Induced by Rogue Waves

Shiyu Lyu, Luofeng Huang, and Giles Thomas

University College London,United Kingdom

Rogue waves are short-lived large amplitude irregular waves that randomly occur in oceans and significantly affect the safety of marine structures. Most past research has focused on the formation of rogue waves and their interaction with fixed marine structures; in contrast, research on their interactions with freely floating structures is somewhat lacking. This paper outlines work conducted to simulate the motions of a floating structure induced by rogue waves based on OpenFOAM. Code development has included the generation of a rogue wave group and its incorporation with the overset mesh technique to allow a large displacement of the structure. Validation of the developed code has been conducted through comparing the motions of a floating body in regular waves with existing experimental data. Investigations were then performed on the motions of the same floating body with different degrees of freedom induced by rogue waves. The behaviour of the floating body is analysed in detail; for example, the sway, heave and the persistent roll motions after the wave has hit the structure. In addition, the numerical results of forces and moments of the moving body are compared with their fixed counterparts.

1 Introduction

Rogue waves, also known as freak waves, containing large crests and deep troughs randomly appear in the ocean, which usually induce the peak load on marine structures. There has been extensive research on the propagation of the rogue or freak waves, based on a focused waves group generated using linear wave theory or second-order stokes theory [1]. Ning et al. [2] studied the shift distance of focal point with the increase of wave nonlinearity through using the focused wave group in a fully nonlinear numerical tank. Vyzikas et al. [3] validated the surface elevation of the focused waves using OpenFOAM against the measured values and further investigated the individual evolution of high order terms. Studies on the interaction of the rogue waves with fixed structures have also been conducted by many researchers, where numerical results show a good agreement with the experimental data. For instance, Chen et al. [4] performed focused waves impact on a bottom-mounted vertical cylinder based on OpenFOAM with up to 4th order harmonics captured accurately. Hu et al. [5] predicted the surface elevation and the pressure in front of a fixed FPSO in extreme waves using OpenFOAM with good accuracy and efficiency. Abdussamie et al. [6] predicted the impact forces and slamming pressure on a fixed multicolumn offshore platform in extreme wave event and found that the numerical results are in good agreement with the measured data. Although some success has been achieved, the rogue wave-induced forces and motions have not been thoroughly investigated, due to the complexity of the inherent mechanism of rogue waves [7]. Moreover, most of the studies have focused on the formation of rogue waves and their interaction with fixed marine structures, further investigation on their interactions with freely floating structures is needed.

One challenge of modelling the interaction of rogue waves with a floating structure is to handle the dynamic mesh, as a large movement of the structure is expected to happen with such an extreme wave condition. In this kind of simulation, the quality of dynamic meshes is difficult to preserve by using the traditional method that only allows small mesh deformations. Thus, this work incorporates the overset mesh functionality in OpenFOAM to handle the large structural movement. Validation

of the developed code is first conducted to the motions of a floating body in regular waves. Then, investigations are performed on the motions of the same floating body induced by rogue waves.

2 Numerical approach

2.1 Computational domain and boundary conditions

A two-dimensional rectangular computational domain is established, as shown in Figure 1a, defined by the Cartesian x-z coordinate system. The length and water depth of the numerical water tank are consistent with the corresponding experiments [5, 8], i.e. $18m$ long and $0.4m$ water depth for the regular wave case; $18m$ long and $2.93m$ water depth for the irregular rogue wave case. For all simulations presented in this paper, a homogeneous rigid body is initially half-immersed in still water with the density of $500kg/m^3$, the breadth of $0.3m$ and the height of $0.2m$. The no-slip wall boundary condition is applied for the seabed and the floating body surface. The top boundary is defined as a static pressure boundary condition to represent the total pressure of atmospheric is equal to static pressure.

The relaxation zone method in the waves2Foam toolbox [9] is used to work simultaneously with wave generation at the inlet and wave absorption at the outlet. At the wave generation zone, waves are generated based on the analytical values of the velocity field and free surface, which are used to initiate the numerical computation. At the wave dissipation zone, velocity and free surface are damped smoothly to approach zero and the still water level, respectively, which guarantee that there is almost no reflection of wave back into the computational domains.

In this study, the velocity input boundary conditions are implemented to generate the regular and irregular rogue waves at the inlet zone based on the linear Stokes' wave theory [10] and NewWave theory [11], respectively. The free surface elevation of rogue wave can be obtained by the summation of linear regular wave components,

$$\eta(x,t) = \sum_{n=1}^{N} a_n \cos\left(k_n(x-x_0) - \omega_n(t-t_0) + \varepsilon_n\right) \tag{1}$$

where x_0 and t_0 are the focused position and time, ω_n is the circular frequency of the nth wave component, k_n is the wave number of the nth wave which can be computed based on dispersion relation for the given value of water depth d, $k_n = {\omega_n}^2/[g\tanh(k_n d)]$, and ε_n is the random initial phase. Each wave components have adjusted initial phase so that a large amount of energy is focused at the position x_0 for time t_0. That is $\cos(k_n(x-x_0) - \omega_n(t-t_0) + \varepsilon_n) = 1$ and hence $\varepsilon_n = 2\pi m, m = 0, 1, 2, ...$

The amplitude of the nth wave component can be expressed as,

$$a_n = A_f \frac{S(\omega_n)\cdot\Delta\omega}{\sum\limits_{N} S(\omega_n)\cdot\Delta\omega} \tag{2}$$

where A_f is the target linear amplitude of focused waves group, $S(\omega_n)$ is the spectral density of JONSWAP spectrum [12] and $\Delta\omega = (\omega_{max} - \omega_{min})/N$ is angular frequency step depending on the bandwidth $\omega_{max} - \omega_{min}$ and the number of wave components N.

The velocity profiles of rogue waves group are calculated by summing the velocity of regular wave components,

$$u = \sum_{n=1}^{N} a_n\omega_n \frac{\cosh(k_n(z+d))}{\sinh(k_n d)}\cos(\varphi_n) \tag{3}$$

$$w = \sum_{n=1}^{N} a_n\omega_n \frac{\sinh(k_n(z+d))}{\sinh(k_n d)}\sin(\varphi_n) \tag{4}$$

where u and w are the horizontal and vertical component of velocity, respectively; d is water depth from the seabed to still water level, z is vertical coordinate to describe wave motion in which $z = 0$ is the still water level.

2.2 Computational method

The flow fields are governed by the Navier-Stokes equations for an incompressible Newtonian fluid. The interface between water and air is captured by solving the volume fraction equation, namely volume of fluid method [13]. By applying the Finite Volume method [14], the numerical solution of the governing equations can be obtained through domain discretisation and equation discretisation. The mesh density for the background meshes and overset meshes in this study is selected by sensitivity tests. Also, adjustable timestep in OpenFOAM is used to accelerate the computational speed with a max Courant number of 0.25 [15]. Each timestep can automatically adjust according to instantaneous velocity and cell size, which can achieve better computational efficiency than using a uniform timestep.

In contrast to the single-block dynamic deforming mesh, the overset mesh technique uses a collection of generated overlapping meshes and appropriate interpolation scheme to build a composite and continuous computational domain, as shown in Figure 1b. The meshes for the floating body and background are generated independently and assembled together. Then all the cells are scanned and identified as different types [16]. Cells located

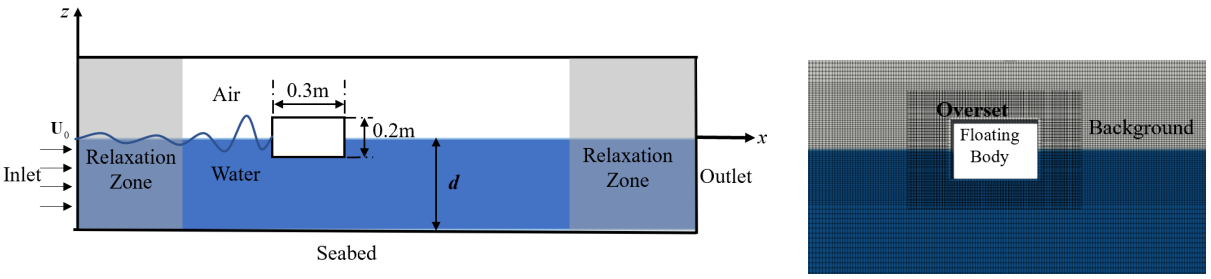

(a) (b)

Figure 1: (a)Layout of the numerical wave tank: a rectangular body floating on the free surface and subjected to incoming waves; (b)Profile of computational domain of the overset grid mesh: the background mesh is refined around the free surface and the floating body

inside the region of the floating body are marked as holes and excluded from the computation. The receptor or fringe cells surrounding the holes are treated as boundaries of the overset meshes to exchange the information between the component meshes. The donor cells are selected from background meshes to provide the flow information for the receptor cells. Specifically, the value of a variable of the receptor cell which can be velocity or pressure is obtained by interpolation from the donor cells,

$$\phi = \sum_{i=1}^{n} \omega_i \cdot \phi_i \tag{5}$$

where ω_i is the weight coefficient $\sum_{i=1}^{n} \omega_i = 1$ and ϕ_i is the ith donor cell value. In this study, the inverse distance interpolation scheme is performed by $\phi = \sum_{i=1}^{n} \frac{\phi_i}{r_i} / \sum_{i=1}^{n} \frac{1}{r_i}$ in which r_i is the distance between donor cells and the fringe cell.

In order to obtain the solution in the whole computational domain, the global matrix needs to be assembled by correcting the off-diagonal elements, which are taking into account the presence of holes in the background meshes and providing appropriate coupling between background and overset meshes. Finally, the motions of the rigid body are obtained by solving the equation of motions in which the forces and moments are obtained by integrating the pressure and viscous forces over the wet surface of the floating rigid body.

3 Results and Discussion

In this section, validation of the generated regular waves and regular wave-induced body motions are presented against the experiments of He et al. [8]. Subsequently, the wave condition is changed to a rogue wave group [5], and the hydrodynamic response of the floating body is studied.

3.1 Validation

The sway, heave and roll motions of a floating body has been simulated when facing the regular waves with different wave height ($H = 0.04m$ and $H = 0.10m$) and same wave period ($T = 0.12s$) in the wave flume. A reference system 0-xz is defined, with x position rightwards and z positive upwards. ϕ donates the roll angle which is positive in the clockwise direction. From Figure 2 and 3, the incoming regular wave with wave height $0.04m$ and $0.10m$ is seen to be well reproduced by numerical simulation according to the wave elevation. It also can be seen that the present numerical simulations of regular wave-induced motions in all three degrees of freedom are agreed well with the experimental data from He et al. [8]. Figure 4 shows the centroid trajectories of the freely floating body in a motion period under the regular waves with different amplitudes. The numerical results and the corresponding experimental data [8] are in good agreement. Thus, the overset grids technique can be used to compute the floating body subjected to large amplitude waves, which overcomes the limitation of the dynamic mesh without topology change.

3.2 A floating body in rogue waves

The generation of rogue waves is validated by comparing the wave elevation at the focal point with experimental data [5].The irregular waves group with wave components N=30, peak wave period $T_p = 1.456s$, peak wavelength $\lambda_p = 3.31m$ and target linear amplitude $A_f = 0.103m$ in the frequency band 0.1-2.0Hz is implemented in the inlet boundary. In addition, the linear focal point x_0 and focus time t_0 are specified as $1.5\lambda_p$ and $8T_p$, respectively. As shown in Figure 5, the wave elevations are obtained from three uniform meshes with $\Delta x = 0.06, \Delta z = 0.02$(Mesh a), $\Delta x = 0.02, \Delta z = 0.01$(Mesh b), and $\Delta x = 0.01, \Delta z = 0.005$(Mesh c). When compared with the experimental data, the results of Mesh b and c are identical and give

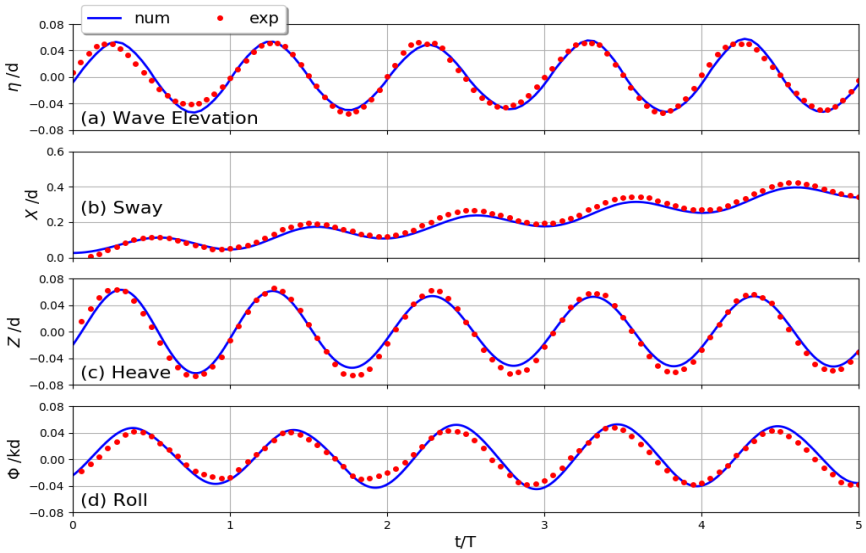

Figure 2: Sway, heave and roll response of the floating body due to an incoming regular wave with $H = 0.04m$ (The time is normalised by the incoming wave period ($T = 1.2s$). The heave and the sway are normalised by the water depth ($d = 0.4m$) and the roll by the wavenumber multiply by the water depth.).

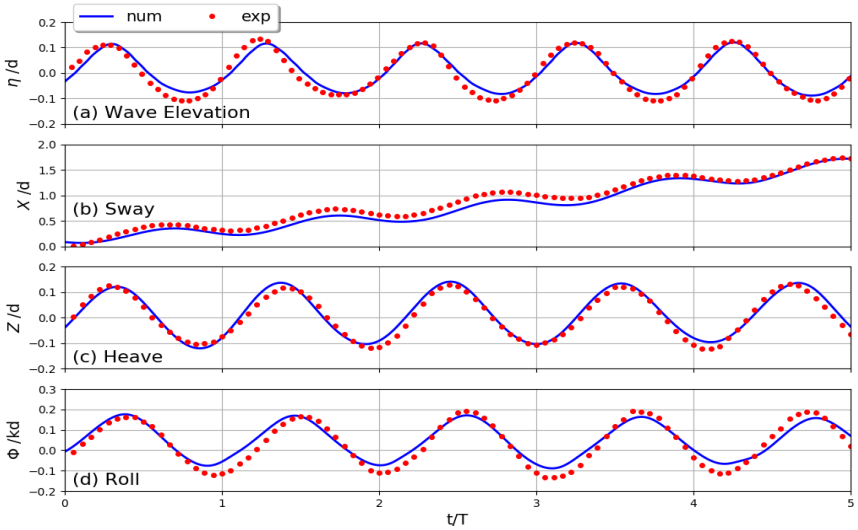

Figure 3: Sway, heave and roll response of the floating body due to an incoming regular wave with $H = 0.10m$.

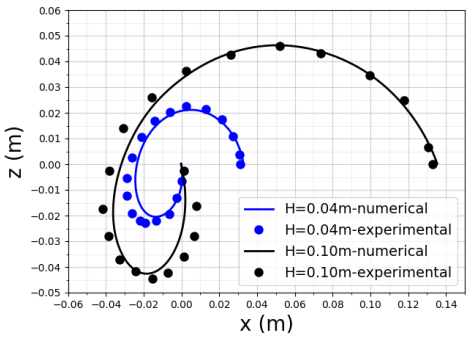

Figure 4: The centroid trajectories of the floating body in one motion period.

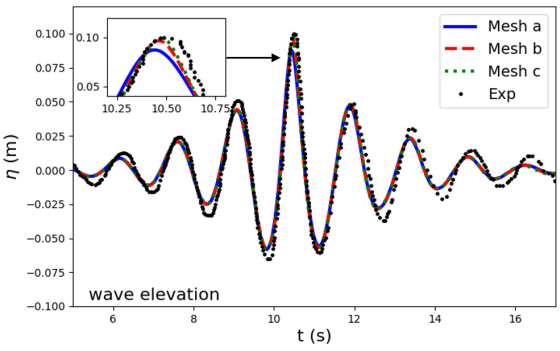

Figure 5: Time series of incident wave surface elevation at the actual focus point.

an improvement on the maximum crest than that of Mesh a. Considering the computational efficiency, Mesh b that provided mesh convergence results is used in later simulations. Then, the floating body is subjected to generated rogue waves, with different degree(s) of freedom (DoF) enabled in a two-dimensional numerical wave tank. The front edge of the floating body is located exactly at the actual focal point of the focused waves group. The 3-DoF and 0-DoF cases describe the rigid body undertaking freely motion and being fixed in the waves, respectively, while the 2-DoF case represents the body with only the sway mode restricted.

The translations in x-axes and z-axes directions, as well as rotation about y-axes direction of 3-DoF and 2-DoF cases, are presented in Figure 6. A large total drift motion can be seen in 3-DoF case. In addition, several oscillatory motions are also visible in the x-direction due to the fact that there are several peaks in this wave mode. For the heave motion in the Figure 6(b), the floating body is lifted with several relatively large peaks at the time of the wave peaks arriving. This is because there is a restoring force along the z-axis as a result of the difference in gravity and buoyancy. The heave motions of 3-DoF and 2-DoF are almost identical since both cases are free along z-axes. For the rotation about the y-axis, the floating body in both cases is undergoing roll motion with several relatively large peaks in the irregular waves. Besides, the oscillation of the rotation is most obvious in Figure 6(c), which means that it is more persistent and has a lower decay rate when compared with the translations. This is due to the disturbance of rotation being relatively small, as the rotation centre is on the mean free surface. Another possible reason is that the resonance of roll motion is excited by the focused waves group since the peak frequency ($f_p = 0.69Hz$) is close to the roll natural frequency ($f_n = 0.66Hz$). The natural frequency for the roll motion is based on the experiment of free roll decays of this floating box in still water [8]. Moreover, the amplitude of roll motion in 2-DoF case is much larger and shown a little forward in time when comparing the motion in 3-DoF. The reason for this phenomenon is the relative motion between the wave and the floating body. It requires extra time for the forward travelling wave group to reach the position of the freely moving body due to the drift motion.

Figure 7 gives the time history of the forces and moments acted on the fixed body, the body with free motion and the body with restrained sway motion. The horizontal forces in the case of the freely moving floating body are much smaller than those on the fixed one and the one with 2-DoF, as can be observed from Figure 7(a), which shows the body motions can release the loading from incoming waves. From Figure 7(b), the vertical forces on the freely moving body and the body moving with sway motion restrained are almost the same, which are much smaller than the force on fixed one. It can be also seen from Figure 7(c) that the moment oscillates for a long period after the irregular wave group have well cleared off the floating body with two or three degrees of freedom, while the moment for the fixed body approaches zero immediately when the wave has moved away. Furthermore, the vertical force and moment show some fluctuations after a big crest has passed in the 0-DoF cases, which is due to the occurring of wave overtopping.

4 Conclusions

This study combines the NewWave theory [11] with the overset mesh technique to simulate the motions of a floating body in rogue waves. The overset mesh technique reveals good accuracy and flexibility in predicting the hydrodynamic response of a floating body. It has been found that the loading on a floating body is much smaller than that of the fixed one, which is attributed to the wave energy released by the body motions, namely, more degrees of freedom of a floating body appear to decrease the peak impact pressure. It has also been found that the moment oscillates for a long period even after the rogue wave group has cleared well away from the moving body, because of the rotational motion which is persistent and decays slowly, while the moment for the fixed body approaches zero immediately when the wave has passed. Future work could be extended to the three-dimensional case with 6 degrees of freedom. Some specific behaviours can also be further investigated, such as green water [17].

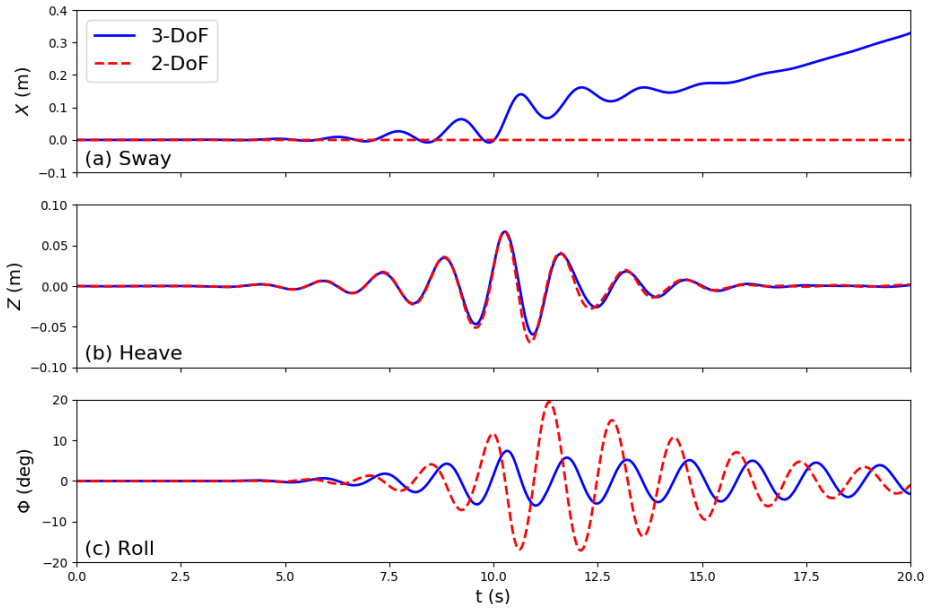

Figure 6: Time history of motions of the floating body subjected to the rogue waves: (a) displacement in the horizontal x-direction; (b) displacement in the vertical y-direction; (c) rotation displacement.

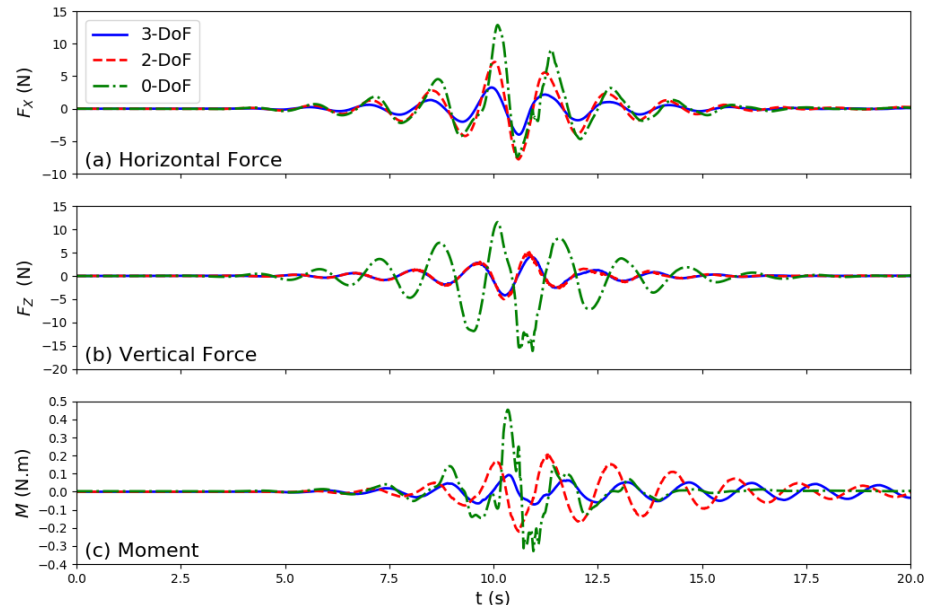

Figure 7: Time history of wave forces and moments of the moving and fixed floating body subjected to the rogue waves.

References

[1] JF Dalzell. A note on finite depth second-order wave–wave interactions. *Applied Ocean Research*, 21(3):105–111, 1999.

[2] DZ Ning, J Zang, SX Liu, R Eatock Taylor, B Teng, and PH Taylor. Free-surface evolution and wave kinematics for nonlinear uni-directional focused wave groups. *Ocean Engineering*, 36(15-16):1226–1243, 2009.

[3] Thomas Vyzikas, Dimitris Stagonas, Eugeny Buldakov, and Deborah Greaves. The evolution of free and bound waves during dispersive focusing in a numerical and physical flume. *Coastal Engineering*, 132:95–109, 2018.

[4] LF Chen, J Zang, AJ Hillis, GCJ Morgan, and AR Plummer. Numerical investigation of wave–structure interaction using openfoam. *Ocean Engineering*, 88:91–109, 2014.

[5] Zheng Zheng Hu, Deborah Greaves, and Alison Raby. Numerical wave tank study of extreme waves and wave-structure interaction using openfoam®. *Ocean Engineering*, 126:329–342, 2016.

[6] Nagi Abdussamie, Roberto Ojeda, Yuriy Drobyshevski, Giles Thomas, Walid Amin, et al. The impact of extreme wave events on a fixed multicolumn offshore platform. *International Journal of Offshore and Polar Engineering*, 27(03):293–300, 2017.

[7] Christian Kharif and Efim Pelinovsky. Physical mechanisms of the rogue wave phenomenon. *European Journal of Mechanics-B/Fluids*, 22(6):603–634, 2003.

[8] Ming He, Bing Ren, and Da-hong Qiu. Experimental study of nonlinear behaviors of a free-floating body in waves. *China Ocean Engineering*, 30(3):421–430, 2016.

[9] Niels G Jacobsen, David R Fuhrman, and Jørgen Fredsøe. A wave generation toolbox for the open-source cfd library: Openfoam®. *International Journal for numerical methods in fluids*, 70(9):1073–1088, 2012.

[10] John Nicholas Newman. *Marine hydrodynamics*. MIT press, 2018.

[11] Peter S Tromans, Ali R Anaturk, Paul Hagemeijer, et al. A new model for the kinematics of large ocean waves-application as a design wave. In *The First International Offshore and Polar Engineering Conference*. International Society of Offshore and Polar Engineers, 1991.

[12] Yoshimi Goda. A comparative review on the functional forms of directional wave spectrum. *Coastal Engineering Journal*, 41(1):1–20, 1999.

[13] Cyril W Hirt and Billy D Nichols. Volume of fluid (vof) method for the dynamics of free boundaries. *Journal of computational physics*, 39(1):201–225, 1981.

[14] Henk Kaarle Versteeg and Weeratunge Malalasekera. *An introduction to computational fluid dynamics: the finite volume method*. Pearson education, 2007.

[15] Richard Courant, Kurt Friedrichs, and Hans Lewy. On the partial difference equations of mathematical physics. *IBM journal of Research and Development*, 11(2):215–234, 1967.

[16] ZH Ma, L Qian, PJ Martinez-Ferrer, DM Causon, CG Mingham, and W Bai. An overset mesh based multiphase flow solver for water entry problems. *Computers & Fluids*, 172:689–705, 2018.

[17] Inno Gatin, Nikola Vladimir, Šime Malenica, and Hrvoje Jasak. Green sea loads in irregular waves with finite volume method. *Ocean Engineering*, 171:554–564, 2019.